Tones in the acoustic far field of jets in the upstream direction

Christophe Bogey

Tones in the acoustic far field of jets in the upstream direction

Christophe Bogey*
Laboratory of Fluid Mechanics and Acoustics, LMFA UMR 5509, 69130 Ecully, France

The presence of tones in the acoustic far field of isothermal round jets for angles $\phi \geq 120^o$ relative to the flow direction is investigated for Mach numbers between M = 0.60 and 2 based on data from both experiments and large-eddy simulations. For all Mach numbers, as observed in the jet near-nozzle region in previous studies, peaks are found in the far-field pressure spectra regardless of the nozzle-exit boundary-layer properties. They emerge near the cutoff frequencies of the free-stream upstream-propagating guided jet modes, predicted by a vortex sheet model, sharply for M $\geq$ 0.90 but more weakly for lower Mach numbers. The variations of their characteristics with the radiation angle are shown. As the angle increases, the peaks are more prominent, and the most apparent ones are related to lower azimuthal modes. Thus, peaks associated with the axisymmetric mode strongly predominate in the upstream direction.

Nomenclature

c	=	speed of sound
D	=	nozzle diameter
f	=	frequency
L	=	extent of the computational domain
M	=	Mach number, u_j/c_a
N	=	number of grid points
n	=	mode number
p	=	pressure
R	=	distance from the nozzle exit
r_0	=	nozzle radius, $D/2$
(r, θ, z)	=	cylindrical coordinate system
St_D	=	diameter-based Strouhal number, fD/u_j
T	=	temperature
u_j	=	jet velocity at the nozzle exit

*CNRS Research Scientist, Univ Lyon, Central School of Lyon (ECL), INSA Lyon, Univ Claude Bernard Lyon I, christophe.bogey@ec-lyon.fr, Associate Fellow AIAA.

δ_{BL} = thickness of Blasius boundary-layer profile

δ_θ = momentum thickness

ν = kinematic molecular viscosity

ρ = density

ϕ = angle relative to the flow direction

$\langle\rangle$ = temporal averaging operator

Subscript

a = ambient conditions

Superscript

$'$ = fluctuation

I. Introduction

For the last six decades, the characteristics of jet noise components have been determined most often based on measurements made in the acoustic far field, where the root-mean-square values of pressure fluctuations vary as the inverse of the distance from the nozzle exit. The broadband shock-associated noise and screech noise, emitted by shock-containing jets in the sideline and upstream directions, have been investigated from far-field data acquired for large angles ϕ relative to the flow direction, such as $\phi = 150^o$ in Norum and Seiner [1] and $\phi = 175^o$ in Norum [2], for instance. The mixing noise components, radiated by all jets predominantly in the downstream direction, have been studied for smaller angles, typically of $\phi = 30^o$ and 90^o as in Zaman and Yu [3]. For jets generating only mixing noise, including subsonic jets, far-field spectra and directivities have thus been usually obtained over a limited range of angles. For example, they are provided for $\phi \leq 105^o$ in Lush [4], $\phi \leq 120^o$ in Mollo-Christensen et al. [5] and Ahuja and Bushell [6], $\phi \leq 130^o$ in Brown and Bridges [7] and Tam et al. [8] and $\phi \leq 135^o$ in Tanna [9]. Unfortunately, to the best of the author's knowledge, no measurements are available for larger angles. This lack of data can also be attributed to the fact that due to the weak sound levels in the upstream direction at low Mach numbers, the pressure signals might be contaminated by extraneous noise or undesired reflections, possibly causing spurious oscillations in the spectra [10]. This issue likely led some researchers to disregard tones emerging in the sound spectra of subsonic jets in the past.

Despite these difficulties, the presence and physical nature of acoustic tones in the near-nozzle region of high-speed jets have recently been recognized. These tones were documented for the first time by Suzuki and Colonius [11]

for jets at Mach numbers close to 0.9. Their origin, properties and persistence at lower and higher Mach numbers were later investigated by Towne et al. [12], Brès et al. [13] and Bogey [14], among others. The emergence of the tones was shown to be related to the existence of guided jet waves, essentially confined inside the jet core. These waves, discovered by Tam and Hu [15] and sometimes called as neutral acoustic waves in the literature, have gained renewed interest over the last years. In particular, a number of studies revealed their role in the establishment of feedback mechanisms in jets [16–20], refer also to the review paper of Edgington-Mitchell [21]. Towne et al. [12] demonstrated that for $M \gtrsim 0.80$, some of the upstream-propagating guided jet waves can have resonant interactions with downstream-propagating ones, leading to the presence of trapped waves in the jet core. They also proposed to separate the guided jet waves into two categories, namely the the duct-like and the free-stream waves. The first ones are entirely confined inside the jet, whereas the second ones have a significant radial support outside, thus contributing to the jet near pressure field. The free-stream upstream-propagating guided jet waves are also allowed only over narrow frequency bands. For $M \gtrsim 0.80$, the waves cannot exist above the band upper limit, whereas for lower Mach numbers, their magnitudes decay gradually with the frequency around the band limit, resulting in sharp and smooth cutoffs, respectively [14].

The footprints of the guided jet waves in the acoustic far field of high subsonic jets have been explored using experiments in Jaunet et al. [22] and Zaman and Fagan [23] and large-eddy simulations (LES) in Bogey [14]. Jaunet et al. [22] reported significant coherence levels between the near-nozzle tones and the sound waves at 30 nozzle diameters from the jet exit at high polar angles for Mach numbers close to 0.82. Zaman and Fagan [23] noticed the presence of undulations in the spectra measured at 25 diameters and an angle of 60° for jets at Mach numbers typically between 0.90 and 1 at diameter-based Strouhal numbers around 1.5, resembling those in the near-nozzle spectra. Given the non anechoic arrangement in their experiments, they made the hypothesis that the undulations are due to reflections by some uncovered surfaces in the vicinity of the nozzle. In Bogey [14], for a jet at a Mach number of 0.90, no acoustic tone was found to emerge in the far field spectra for radiation angles lower than 135°. Tones similar to the near-nozzle tones were however detected for higher angles. Unfortunately, the spectra were calculated only up to the angle of $\phi = 165°$. No far-field results were also given for jets at other Mach numbers.

In this paper, in order to fill in the lacks highlighted above, the presence of tones in the acoustic far field of isothermal jets is investigated for large radiation angles up to $\phi = 180°$ over a wide range of Mach numbers. For that purpose, far-field data from both experiments and LES are considered. The experimental data are taken from a database built up fifteen years ago [24], getting access to the far-field sound spectra and directivities for jets at Mach numbers between 0.60 and 1.10 up to the angle $\phi = 150°$. The spectra at $\phi = 150°$ are specifically examined in the present paper based on the current knowledge on the near-nozzle acoustic tones and upstream-propagating guided jet modes. As for the simulation data, they come from recently performed LES of jets at Mach numbers between 0.60 and 2, for which the near-nozzle tones have just been described [14]. In practice, the jet acoustic near fields obtained by LES are propagated

to the far field for angles $\phi \geq 120^o$ using the linearized Euler equations. The effects of the nozzle-exit flow conditions on the tones appearing in the spectra will be briefly addressed. More importantly, the variations with the radiation angle of the tone properties, in terms of strength, prominence and associated azimuthal and radial mode numbers, will be discussed up to $\phi = 180^o$.

The paper is organized as follows. The experimental and computational results are presented in sections II and III, respectively. Concluding remarks are given in section IV. Finally, spectra obtained for an experimental jet at a Mach number of 0.90 for radiation angles between $\phi = 30^o$ and 150^o are provided in an appendix.

II. Experimental results

A. Jet parameters and experimental set-up

The experimental data reported in the present paper have been obtained in a former work carried out in the high-speed anechoic wind tunnel of the Centre Acoustique at Ecole Centrale de Lyon. In that work, measurements were performed in the near and far pressure fields of isothermal and cold round jets with the main aim of creating a database for the validation of jet noise LES, refer to the associated article [24] for details on the jet conditions and the experimental set-up.

Five isothermal round jets, exhausting from a converging nozzle of exit diameter $D = 38$ mm, are considered. They have Mach numbers equal to $M = u_j/c_a = 0.60$, 0.75, 0.90, 0.98 and 1.10 and Reynolds numbers $Re_D = u_j D/\nu$ varying between 5.3×10^5 and 9.7×10^5, where u_j is the nozzle-exit velocity in the subsonic cases and the equivalent fully expanded jet velocity in the supersonic case, and c_a and ν are the speed of sound in the ambient medium and the kinematic molecular viscosity. Given their Reynolds numbers, they can be assumed to be initially highly disturbed according to the experiments of Zaman [25].

For the five jets, pressure signals were acquired using microphones located on an arc centered on the nozzle exit of radius $R = 2$ m or 52.6D, ensuring far-field conditions [26, 27], for radiation angles between $\phi = 10^o$ and 150^o with respect to the flow direction. The microphone boom was wrapped with acoustic lining in order to avoid spurious reflections. In reference [24], the far-field directivities are plotted up to $\phi = 150^o$ and sound pressure spectra are provided up to $\phi = 90^o$ for the jets at M = 0.60, 0.75, 0.90 and 0.98 and up to $\phi = 140^o$ for M = 1.10. The spectra at $\phi = 90^o$ for the subsonic jets are broadband, in agreement with the literature [5, 7–9], while the spectrum at $\phi = 140^o$ for M = 1.10 is dominated by screech tones and broadband shock-associated noise components, as the jet is under-expanded at the exit of the convergent nozzle. The spectra evaluated for the largest angle permitted by the microphone arc, namely $\phi = 150^o$, were not shown, most probably because they contain some peaks whose origin was unknown.

B. Far-field sound pressure spectra at an angle of 150 degrees

The sound pressure spectra obtained at $\phi = 150^{o}$ for the five jets are represented in figure 1(a-e) as a function of Strouhal number $\mathrm{St}_D = fD/u_j$, where f is the frequency. They are scaled in amplitude at a distance of $R = 75D$ from the nozzle exit using the inverse square law. As was done in Bogey [14] for both near-nozzle and far-field spectra, the cutoff Strouhal numbers of the modes ($n_\theta = 0 - 8$, $n_r = 1$) of the free-stream upstream-propagating guided jet waves, where n_θ and n_r are the azimuthal and radial mode numbers, are indicated by dash-dotted lines. The allowable frequency band of the upstream-propagating guided jet waves for mode ($n_\theta = 0$, $n_r = 2$) is also highlighted in grey in figure 1(e) for M = 1.10. The cutoff Strouhal numbers and allowable bands of the modes are obtained from the dispersion relations of the guided jet waves predicted using a vortex-sheet model. In particular, for a given mode, the cutoff frequency is reached at the stationary point associated with a local maximum in the dispersion curve, when this point exists, as is most often the case for M $\gtrsim$ 0.80. This point corresponds to a saddle point in the complex wavenumber space according to Towne et al. [12]. When the dispersion curve has no stationary points, typically for lower Mach numbers, the cuttoff frequency of the free-stream upstream-propagating guided jet mode is approximated by the frequency obtained at the inflexion point of the curve [14].

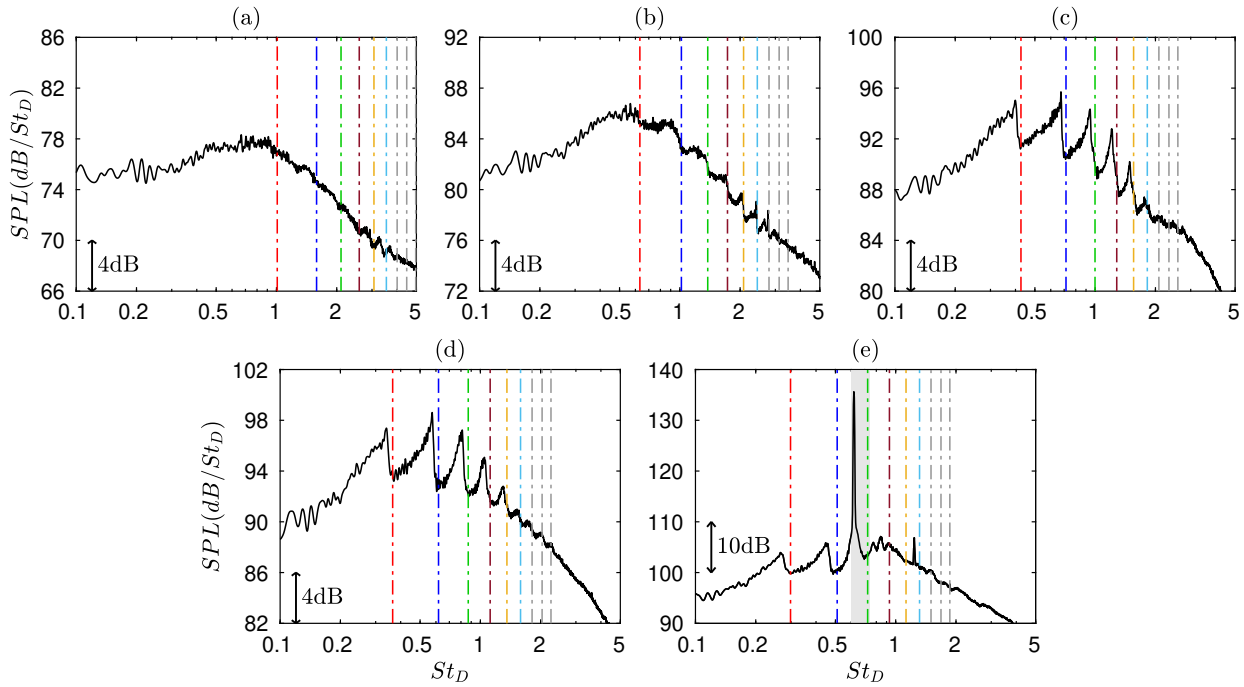

Fig. 1 Sound pressure levels at $\phi = 150^{o}$ for (a) M = 0.60, (b) M = 0.75, (c) M = 0.90, (d) M = 0.98 and (e) M = 1.10; (dash-dotted) cutoff frequencies of the free-stream guided jet modes ($n_\theta =$ 0, 1, 2, 3, 4, 5, 6, 7 and 8, $n_r = 1$); (grey) band for mode ($n_\theta = 0$, $n_r = 2$).

For M = 0.90 and 0.98, in figure 1(c,d), five or six strong peaks emerge in the spectra. The ith peak reaches its maximum level and then decreases sharply very near the cutoff frequency of the mode ($n_\theta = i - 1$, $n_r = 1$) of the free-stream upstream-propagating guided jet waves. For the two lower Mach numbers, peaks are also found but they

are much less visible, especially at low frequencies. For M = 0.75, in figure 1(b), the spectrum thus exhibits four broadband oscillations between $\mathrm{St}_D \simeq 0.4$ and 1.6 and three weak peaks for higher Strouhal numbers, close to the cutoff frequencies of modes ($n_\theta = 0-3$, $n_r = 1$) and ($n_\theta = 4-6$, $n_r = 1$), respectively. For M = 0.60, in figure 1(a), similar oscillations and peaks appear but at lower levels. These results resemble those obtained in the nozzle-exit plane of jets at M = 0.60, 0.75 and 0.90 at the radial position $r = 1.5r_0$, where $r_0 = D/2$, in the recent LES study [14]. They show that, for subsonic jets, the presence of free-stream upstream-propagating guided waves over limited frequency band generate acoustic peaks not only near the nozzle but also in the far field at $\phi = 150^\mathrm{o}$.

For the supersonic jet, in figure 1(e), the spectrum displays an intense screech tone and its first harmonic as well as broadband shock-associated noise components, as observed for large radiation angles for shock-containing jets [1]. The fundamental screech tone lies into the frequency band of the upstream-propagating guided jet mode ($n_\theta = 0$, $n_r = 2$), in agreement with previous studies [18–20]. This can be explained by the fact that the feedback loop of the screech mode A1, most likely establishing in the present jet [28], is completed by waves belonging to the guided jet mode mentioned above. Two peaks also appear in the spectrum below the screech tone frequency. Their shapes and locations around the cutoff frequencies of the modes ($n_\theta = 0-1$, $n_r = 1$) of the upstream-propagating guided jet waves look like those of the two first peaks for M = 0.90 and 0.98. Thus, due to the upstream-propagating guided jet waves, the far-field spectrum contains both screech tones and relatively broad acoustic peaks, as was the case for the near-field spectra of the supersonic jets of Zaman and Fagan [23]. For fully expanded nozzle-exit conditions, the screech tones naturally disappear, but the other peaks can be expected to persist [14].

This point, as well as the variations of the properties of the acoustic peaks for $\phi > 150^\mathrm{o}$, are discussed in the next section based on LES data. Finally, it can be noted that far-field spectra obtained for the experimental jet at M = 0.90 for $\phi < 150^\mathrm{o}$ are provided in the appendix. No tone emerge in the spectra for $\phi \leq 120^\mathrm{o}$, as expected. However, small undulations can be detected down to $\phi = 30^\mathrm{o}$, especially around Strouhal number $\mathrm{St}_D = 2$, as was the case in Zaman and Fagan [23]. They may be due to unwanted acoustic reflections in the experiments.

III. Simulation results

A. Jet parameters and numerical methods

The jet acoustic far fields investigated in this paper have been calculated from LES data obtained for isothermal round jets at $\mathrm{Re}_D = 10^5$, for which the near-nozzle tones have recently been analyzed. The jet and LES parameters are detailed in the related paper [14]. The main ones are summarized below.

Six jets with tripped boundary layers and two jets with untripped boundary layers, characterized by highly disturbed or fully laminar nozzle-exit flow conditions, respectively, are considered. They originate at $z = 0$ from a pipe nozzle into a medium at rest at a temperature $T_a = 293$ K and a pressure $p_a = 10^5$ Pa. At the pipe inlet, at $z = -2r_0$, Blasius

laminar boundary-layer profiles of thickness δ_{BL} are imposed for the axial velocity, radial and azimuthal velocities are set to zero, pressure is equal to p_a and temperature is determined by a Crocco-Busemann relation. The tripped jets have Mach numbers M = 0.60, 0.75, 0.90, 1.10, 1.30 and 2, and boundary layers of thickness $\delta_{BL} = 0.15r_0$ at the pipe inlet, leading to a momentum thickness $\delta_\theta \simeq 0.018r_0$ at the outlet. Their boundary layers are forced by adding random low-level vortical disturbances in the pipe [29] with a magnitude adjusted to reach 9% of peak turbulence intensity at the exit. The untripped jets have a Mach number M = 0.90 and pipe-inlet boundary-layer thicknesses $\delta_{BL} = 0.025r_0$ and $0.2r_0$, yielding $\delta_\theta = 0.004r_0$ and $0.024r_0$ at the nozzle exit.

The LES have been performed using an in-house OpenMP-based solver of the three-dimensional filtered compressible Navier-Stokes equations in cylindrical coordinates (r, θ, z), based on finite-difference and Runge-Kutta explicit schemes with low dissipation and low dispersion [30]. A six-order filtering is applied every time step in order to damp grid-to-grid oscillations, but also as an LES subgrid-scale model relaxing turbulent energy from scales at wave numbers close to the grid cutoff wave number while leaving larger scales mostly unaffected [31, 32]. At the grid boundaries, radiation conditions [33] are implemented with the addition of a sponge zone at the outflow. At the inflow and radial boundaries, density and pressure are also brought back close to p_a and ρ_a. No co-flow is imposed.

Except for the jets at M = 1.30 and 2, the jets have been simulated using the same grid in the (r, z) plane, described and referred to as gridz40B in a grid sensitivity study [34]. The grid contains $N_r = 504$ and $N_z = 2048$ points in the radial and axial directions, and extends radially out to $r = L_r = 15r_0$ and axially down to $z = L_z = 40r_0$. The number of points in the azimuthal direction is $N_\theta = 1024$ for the tripped jets and $N_\theta = 512$ and 256 for the untripped jets with $\delta_{BL} = 0.025r_0$ and $\delta_{BL} = 0.2r_0$. The maximum mesh spacing is equal to $0.075r_0$. For an acoustic wave discretized by five points per wavelength, this mesh spacing provides a Strouhal number $\mathrm{St}_D = 8.9$ for M = 0.60, 7.1 for M = 0.75, 5.9 for M = 0.90 and 1.1 for M = 1.10. For the jets at M = 1.30 and 2, the grids consist of $N_r \times N_\theta \times N_z = 572 \times 1024 \times 2412$ points for M = 1.30 and $572 \times 1024 \times 2947$ points for M = 2. They extend radially out to $r = L_r = 15r_0$ and axially down to $r = L_z = 50r_0$ for M = 1.30 and $60r_0$ for M = 2. The maximum mesh spacing is equal to $0.05r_0$, yielding $\mathrm{St}_D = 6.2$ for M = 1.30 and 4 for M = 2 for an acoustic wave with 5 points per wavelength. After a transient period, the LES have been carried out during a time $T = 3,000r_0/u_j$ for the tripped jet at M = 0.90 and the untripped jet with $\delta_{BL} = 0.2r_0$ $T = 1,500r_0/u_j$ for the tripped jet at M = 0.60 and the untripped jet with $\delta_{BL} = 0.025r_0$ and $T \simeq 1,250r_0/u_j$ otherwise. Density, velocity components and pressure have been recorded at several locations specified in reference [35]. The data of interest here include those on the cylindrical surface at $r = L_r$ and the cross sections at $z = -1.5r_0$ and $z = L_z$, stored at a sampling frequency corresponding to $\mathrm{St}_D = 12.8$, with 256 points retained in the azimuthal direction.

In reference [14], far-field spectra were calculated only for the tripped jet at M = 0.90, for radiation angles limited to $\phi = 165^\mathrm{o}$. In the present work, they have been computed for all jets, nearly up to $\phi = 180^\mathrm{o}$. In practice, the jet near-field fluctuations have been propagated to the far field using an in-house OpenMP-based solver of the linearized Euler

equations in cylindrical coordinates based on the same numerical methods as the LES solver [35, 36]. A computation has also been performed using the weakly non-linear Euler equations [37] for the jet at M = 2. The extrapolations are carried out from the LES velocity and pressure fluctuations recorded during time T at $r = L_r$ and at $z = -1.5r_0$ and L_z. The grids used allow us to obtain the pressure waves radiated at $R = 150r_0$ from the nozzle exit between the angles of $\phi = 120^o$ and 179^o relative to the jet direction. In the radial and axial directions, they contain $N_r \times N_z = 2,673 \times 4,401$ points for the jet at M = 2, $2,673 \times 4,201$ points for M = 1.30 and $1,810 \times 2,717$ points for M $\leq$ 1.10. Excluding the 80-point sponge zones implemented at the boundaries, they extend radially from $r = 1.1r_0$ out to $r = 131r_0$ and axially from $z = -151r_0$ down to $z = L_z + 11r_0$, with a mesh spacing of $0.075r_0$ for M $\leq$ 1.10 and $0.05r_0$ for M $\geq$ 1.30. These mesh spacings are identical to those in the LES near field. In the azimuth, the number of grid points is $N_\theta = 256$ for M $\leq$ 1.10 and $N_\theta = 128$ otherwise. In order to alleviate the time-step restriction near the cylindrical origin, the derivatives in the azimuthal direction at the points closest to the axis are evaluated at a coarser resolution than permitted by the grid [38] using 64 points.

B. Snapshot and far-field conditions

In order to illustrate the characteristics of the jet sound field upstream of the nozzle exit, a snapshot of the vorticity norm and of the pressure fluctuations obtained for the tripped jet at M = 0.90 is provided in figure 2. For clarity, only a limited part of the pressure field is shown. The levels of the acoustic waves are highest in the downstream direction and decrease with the radiation angle approximately up to $\phi \simeq 120^o$, as expected [5]. For $\phi \gtrsim 120^o$, on the contrary, the levels appear not to significantly vary with ϕ. More surprisingly, the sound field seems to be better organized than for $\phi \simeq 90^o$, for instance, and exhibits low-frequency waves correlated over large polar angles, propagating predominantly in the upstream direction.

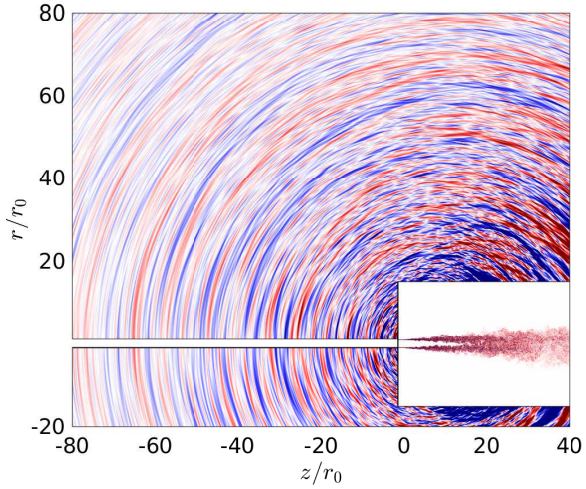

Fig. 2 Vorticity norm and pressure fluctuations for M = 0.90, using colour scales between $\pm 10 u_j/r_0$ and $\pm 1.5 \times 10^{-4} p_a$, from blue to red.

The overall sound pressure levels calculated at $\phi = 150^o$ for the six tripped jets are plotted in figure 3 as a function of the distance R from the nozzle exit using logarithmic scales. Lines are also drawn to represent the inverse square law, indicative of acoustic far-field conditions. The sound levels follow the $1/R^2$ law lines above a minimum distance R increasing with the Mach number, from $R \simeq 80r_0$ for M = 0.60 up to $R \simeq 140r_0$ for M = 2. Therefore, for all jets, the pressure signals obtained at $R = 150r_0$ is acquired in the acoustic far field.

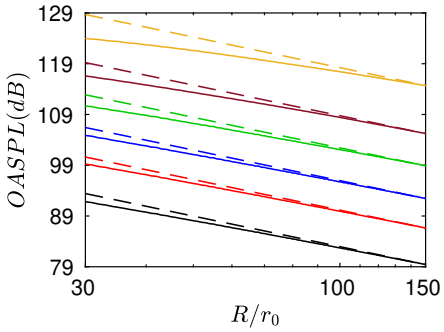

Fig. 3 Overall sound pressure levels at $\phi = 150^o$ for M = ——— 0.60, ——— 0.75, ——— 0.90, ——— 1.10, ——— 1.30 and ——— 2; (dashed) $1/R^2$ law.

In order to finally check that non-linear propagation effects are negligible in this study, the sound spectra determined at $R = 150r_0$ from the nozzle exit for $\phi = 150^o$ and 175^o for the noisiest jet, that is for M = 2, by solving the linearized and the non-linear Euler equations are depicted in figure 4 as a function of the Strouhal number. The spectra obtained using the two sets of equations are superimposed, both for $\phi = 150^o$ where broadband components dominate and for $\phi = 175^o$ where two peaks emerge strongly. This demonstrates that the upstream far-field noise is accurately evaluated using a linear extrapolation method for the present jets.

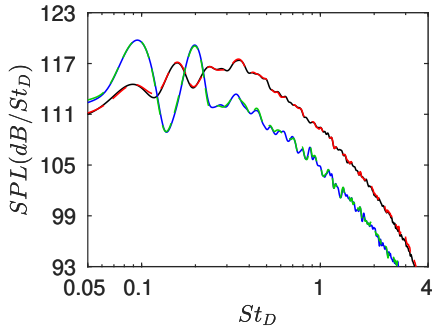

Fig. 4 Sound pressure levels obtained for M = 2 at $\phi = 150^o$ for ——— linear and – – – non-linear propagations and at $\phi = 175^o$ for ——— linear and – – – non-linear propagations.

C. Upstream far-field noise for different nozzle-exit conditions

The sound pressure spectra evaluated at $R = 150r_0$ at $\phi = 150^o$ and $\phi = 175^o$ for the jets at M = 0.90 with untripped boundary layers of thickness $\delta_{BL} = 0.2r_0$ and $\delta_{BL} = 0.025r_0$ and with tripped boundary layers are represented in

figure 5(a-b). The spectra all contain peaks, which are stronger at $\phi = 175^o$ than at $\phi = 150^o$. The peaks are found at the same Strouhal numbers for the three jets despite the wide disparity in boundary-layer thickness and state. In particular, for $\phi = 150^o$ in figure 5(a), the frequencies and shapes of the peaks are comparable to those in the experimental spectrum provided in section II.B for M = 0.90, scaled in amplitude at $R = 150r_0$ using the inverse square law. Therefore, the peaks have the same origin in the simulations and in the experiments. However, the levels and degrees of prominence of the peaks, as well as the levels of the broadband acoustic components, vary appreciably with the jet exit conditions, leading to substantial discrepancies with respect to the measurements. The sound levels are significantly higher for the untripped jets than for the tripped jet, as is the case in the far field at $\phi \leq 120^o$ [34] and in the near-nozzle region [14]. This is expected given the strong additional sound sources in the shear layers of the jets with fully laminar nozzle-exit boundary layers [39]. For the untripped jets, the intensities of the high-frequency peaks are also strengthened relative to those of the low-frequency peaks for a thinner boundary layer.

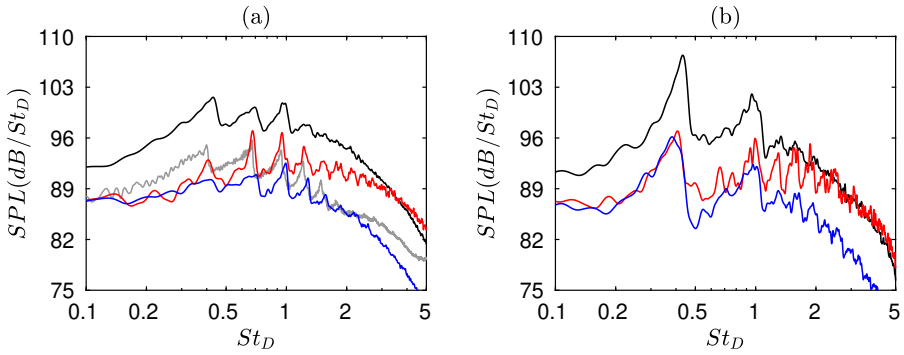

Fig. 5 Sound pressure levels at (a) $\phi = 150^o$ and (b) $\phi = 175^o$ for M = 0.90 jets: untripped ——— thick and ——— thin boundary layers, ——— tripped boundary layers; ——— measurements at $\phi = 150^o$.

The sound spectra at $\phi = 150^o$ and $\phi = 175^o$ are replotted in figures 6(a-c) and 7(a-c), respectively, with the contributions of the first six azimuthal modes. The cutoff Strouhal numbers of the first radial modes of the free-stream upstream-propagating guided jet waves predicted using a vortex-sheet model are also indicated. For M = 0.90, they all correspond to the frequencies at the stationary points associated with local maxima in the dispersion curves [14]. At both angles, the peaks in the spectra are related to the same azimuthal modes for the three jets. As will be discussed in the next subsection, at $\phi = 175^o$, the peaks are associated with lower azimuthal modes than at $\phi = 150^o$. More precisely, they appear at the cutoff Strouhal numbers of the modes ($n_\theta = 0 - 6$, $n_r = 1$) at $\phi = 150^o$, but of the modes ($n_\theta = 0 - 1$, $n_r = 1 - 4$) at $\phi = 175^o$. As a result, at $\phi = 150^o$, the dominant peak is the first peak for $n_\theta = 0$ in figure 6(a) for the untripped jet with $\delta_{BL} = 0.2r_0$, $n_\theta = 1$ in figure 6(b) for the untripped jet with $\delta_{BL} = 0.025r_0$ and $n_\theta = 2$ in figure 6(c) for the tripped jet. At $\phi = 175^o$, the most emerging peak is the first peak for mode $n_\theta = 0$ in all cases, but with respect to the second peak, also for $n_\theta = 0$, it is higher by 6 dB in figure 7(a), 4 dB in figure 7(c) and only 1 dB in figure 7(b).

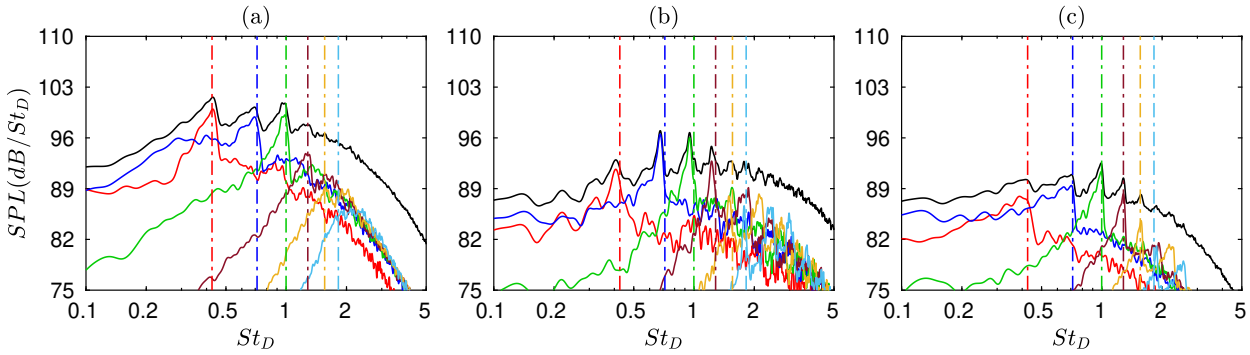

Fig. 6 Sound pressure levels at $\phi = 150^o$ for (a,b) untripped and (c) tripped, M = 0.90 jets: ——— total, n_θ = ——— 0, ——— 1, ——— 2, ——— 3, ——— 4 and ——— 5; (dash-dotted) cutoff frequencies of free-stream guided jet modes ($n_\theta = 0 - 5$, $n_r = 1$).

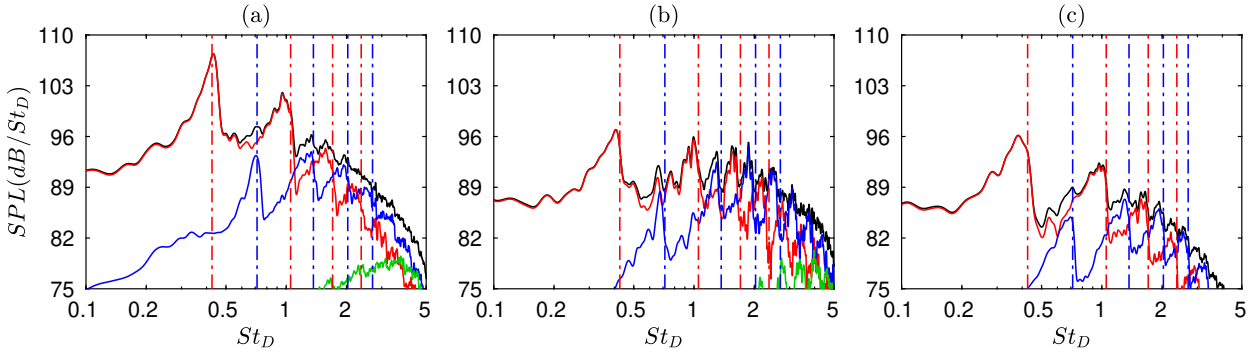

Fig. 7 Sound pressure levels at $\phi = 175^o$ for (a,b) untripped and (c) tripped, M = 0.90 jets: ——— total, n_θ = ——— 0, ——— 1, ——— 2, ——— 3, ——— 4 and ——— 5; (dash-dotted) cutoff frequencies of free-stream guided jet modes ($n_\theta = 0 - 1$, $n_r = 1 - 4$).

D. Upstream far-field noise between Mach numbers 0.60 and 2

The acoustic far fields of the tripped jets at Mach numbers ranging from M = 0.60 to 2 are now explored. For that purpose, the overall sound pressure levels computed at $R = 150r_0$ for M = 0.60, 0.90 and 1.30 are represented in figure 8(a-c) for $\phi \geq 120^o$. The levels calculated for the azimuthal modes $n_\theta = 0$ to 8 are also plotted. The results obtained for the three jets and those for the jets at M = 0.75, 1.10 and 2, not provided for conciseness, are very similar. The total sound levels do not vary much with the radiation angle, displaying a decrease of only approximately 2 dB between $\phi = 120^o$ and 180^o, and the modes $n_\theta = 1$ and 2 are dominant at $\phi = 120^o$, in agreement with the data available in the literature for subsonic jets [13, 24, 40–42]. The variations of the sound levels for the different azimuthal modes at $\phi \geq 135^o$ are less expected, but consistent with preliminary findings of the author [14]. Three trends can be distinguished depending on the mode number. In the first case, encountered for the modes $n_\theta \geq 5$ at M = 0.60 and $n_\theta \geq 6$ at M = 0.90 and 1.10, the levels decrease monotonically with the angle. In the second one, for lower azimuthal modes except for $n_\theta = 0$, they first increase slightly by a 1-2 dB, reach a maximum value, and then fall dramatically by more than 10 dB. The maximum value is achieved near $\phi = 165^o$ for $n_\theta = 1$ and $\phi = 150^o$ for $n_\theta = 2$, for instance. Finally, for the axisymmetric mode, the levels strongly grow up to $\phi = 180^o$, leading to a gain of roughly 8 dB relative to the minimum levels at $\phi \simeq 140^o$. As a result, the mode $n_\theta = 0$ is highly dominant near $\phi = 180^o$, in line with the hypothesis made in reference [14]. These noise directivities are due to the emergence of peaks in the far-field spectra, as will be highlighted below.

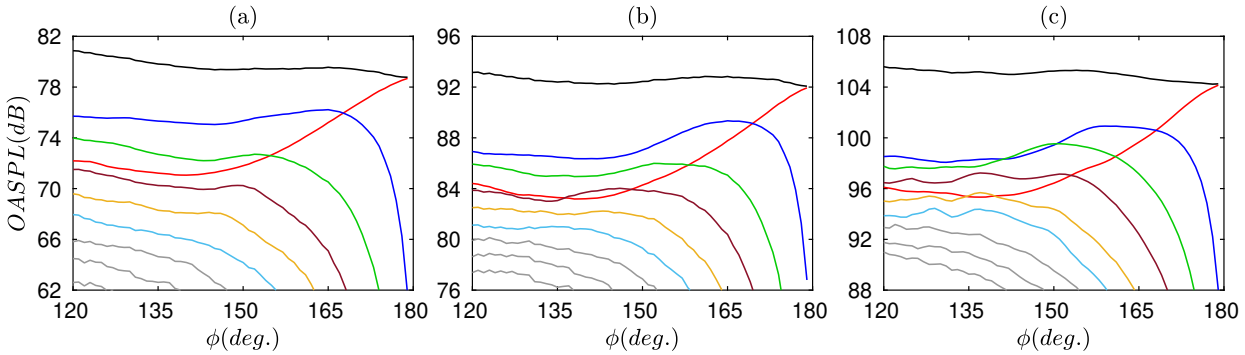

Fig. 8 Overall sound pressure levels for (a) M = 0.60, (b) M = 0.90 and (c) M = 1.30: ——— total, n_θ = 0, 1, 2, 3, 4, 5, 6, 7 and 8.

Before focusing on the peaks, the sound spectra obtained at $R = 150r_0$ and $\phi = 175^o$ for the six jets with tripped boundary layers are represented in figure 9(a) for M = 0.60, 0.75 and 0.90, and in figure 9(b) for M = 1.10, 1.30 and 2. They are normalized, respectively, using the M^8 and M^3 power laws of aerodynamic noise for subsonic jets [43] and supersonic jets [44]. The spectra are broadband for Strouhal numbers $St_D \leq 0.2$ and $St_D \geq 1.5$ in figure 9(a) and for $St_D \geq 1$ in figure 9(b). Over these frequency ranges, they are close to each other, as expected. Outside, they display strong oscillations and peaks, giving rise to significant discrepancies between the curves.

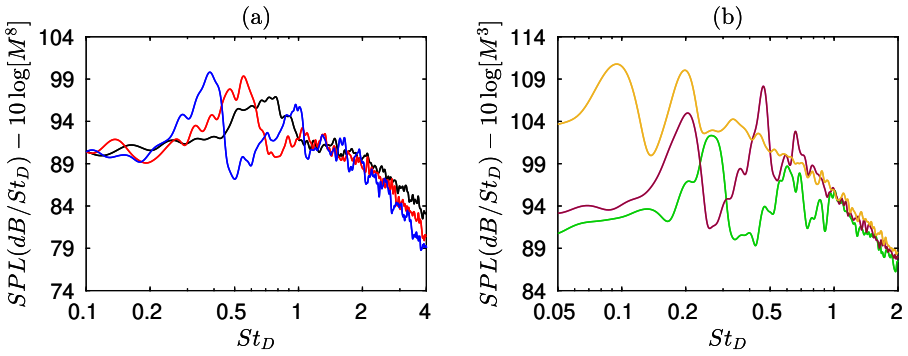

Fig. 9 Sound pressure levels at ϕ = 175° for (a) M = 0.60, 0.75, 0.90 and (b) M = 1.10, 1.30 and 2, normalized using M^8 and M^3 power laws, respectively.

To illustrate the key features of the peaks, the sound spectra evaluated at $R = 150r_0$ at ϕ = 150°, 165° and 175° for the tripped jets are presented in figures 10(a-f), 11(a-f) and 12(a-f), along with the contributions of the first six azimuthal modes. In all cases, peaks are found around the cutoff Strouhal numbers of free-stream upstream-propagating guided jet modes. At ϕ = 150°, in particular, they resemble those in the experimental spectra of section II.B, for the subsonic Mach numbers in figure 10(a-c), but also for M = 1.10 in figure 10(d) despite the higher sound levels and the presence of screech tones in the experiment. They also bear striking similarities with the tonal components obtained near the nozzle exit [14], showing that the latter components propagate to the far field in the upstream direction. However, the peak properties depend significantly on the Mach number and the radiation angle.

Regarding the effects of the Mach number, at the three angles considered, the peaks clearly emerge for M $\geq$ 0.90, with a steep decline on their right side, but they are less prominent and broader for M $\leq$ 0.75 as the Mach number decreases. This can be explained by the characteristics of the guided jet waves over the Mach number range considered [12, 14, 15]. Indeed, for M $\gtrsim$ 0.80, resonant interactions can happen between downstream-propagating and free-stream upstream-propagating guided jet waves [12], whereas they are not possible for M $\lesssim$ 0.80, where downstream-propagating guided jet waves cannot exist according to the vortex-sheet model. Thus, the peaks can be expected to be less marked in the latter case than in the former one. The possibility of resonant phenomena involving upstream-propagating guided jet waves and downstream-propagating disturbances of other nature for M $\lesssim$ 0.80 should however be discussed in future studies. In addition, the allowable bands of the free-stream upstream-propagating guided jet waves widen as the Mach number decreases, and at their upper limits, the cutoff is sharp for M $\gtrsim$ 0.80, whereas for M $\lesssim$ 0.80, it is smooth and occurs at a rate lowering as the jet velocity diminishes [14]. This most likely causes the difference in peak shape and width for the present jets.

As for variations with the radiation angle, overall, the peaks are more visible as the angle approaches ϕ = 180°. They are also associated with lower azimuthal modes. At ϕ = 150°, in figure 10(a-f), peaks are observed for a wide variety of modes from n_θ = 0 to 5, with maximum intensities for n_θ = 1 or n_θ = 2. They are located close to the cutoff

Strouhal numbers of the first radial modes ($n_\theta = 0-5$, $n_r = 1$) of the free-stream upstream-propagating guided jet waves. At $\phi = 165^o$, in figure 11(a-f), two or three strong peaks are seen for both $n_\theta = 0$ and $n_\theta = 1$, as for instance in figure 11(e) for M = 1.30. The peaks are much weaker for $n_\theta = 2$ and negligible for $n_\theta \geq 3$. Lastly, at $\phi = 175^o$, in figure 12(a-f), the predominant peaks are all related to the axisymmetric mode, and lie near the cutoff frequencies of the modes ($n_\theta = 0$, $n_r = 1-3$) of the free-stream upstream-propagating guided jet waves. Thus, at $\phi \geq 135^o$, for modes $n_\theta \geq 1$, acoustic peaks due to the guided jet waves appear, strengthen and then vanish in the far field as the radiation angle increases. The peak strengthening is more marked and the peak maximum levels are reached for a larger angle as the azimuthal mode is lower. For $n_\theta = 0$, the peak growth is even higher than for $n_\theta = 1$ and happens up to $\phi \simeq 180^o$.

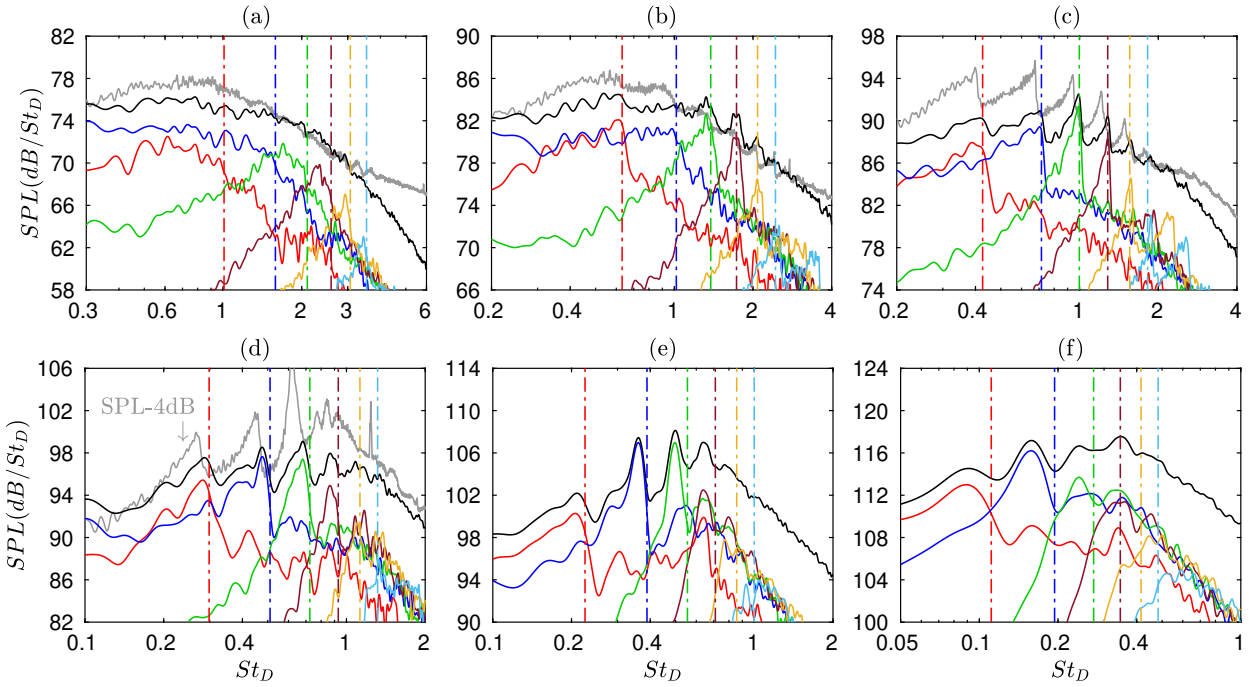

Fig. 10 Sound pressure levels at $\phi = 150^o$ for (a) M = 0.60, (b) M = 0.75, (c) M = 0.90, (d) M = 1.10, (e) M = 1.30 and (f) M = 2: ——— total, n_θ = ——— 0, ——— 1, ——— 2, ——— 3, ——— 4 and ——— 5; ——— measurements; (dash-dotted) cutoff frequencies of free-stream guided jet modes ($n_\theta = 0-5$, $n_r = 1$).

Finally, to further quantify the variations of the peak amplitude with the radiation angle, the sound levels achieved at the peaks associated with the first three radial modes of the free-stream upstream-propagating guided jet waves for $n_\theta = 0-2$ are shown in figure 13(a-c) for $\phi \geq 140^o$ for the jet at M = 0.90. Only the peaks emerging by more than 2 dB with respect to the broadband components are considered. Similar trends are obtained for the other jets. The peak levels all increase up to $\phi \simeq 180^o$ for $n_\theta = 0$, whereas they first grow and then collapse sharply for $n_\theta = 1$ and 2, in agreement with the overall directivities in figure 8(b). Differences can however be noted depending on the radial mode number n_r. As this number increases, the peak levels begin to rise, and reach their maximum values, when they

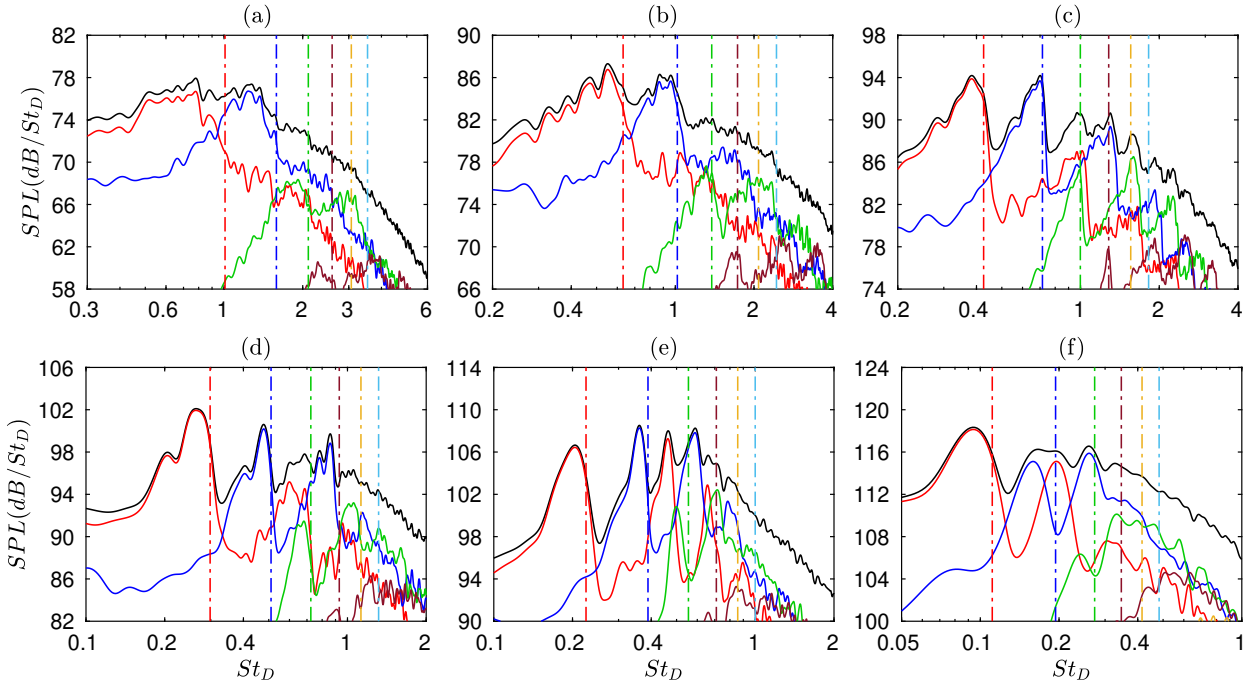

Fig. 11 Sound pressure levels at ϕ = 165° for (a) M = 0.60, (b) M = 0.75, (c) M = 0.90, (d) M = 1.10, (e) M = 1.30 and (f) M = 2: ——— total, n_θ = ——— 0, ——— 1, ——— 2, ——— 3, ——— 4 and ——— 5; (dash-dotted) cutoff frequencies of free-stream guided jet modes (n_θ = 0 – 5, n_r = 1).

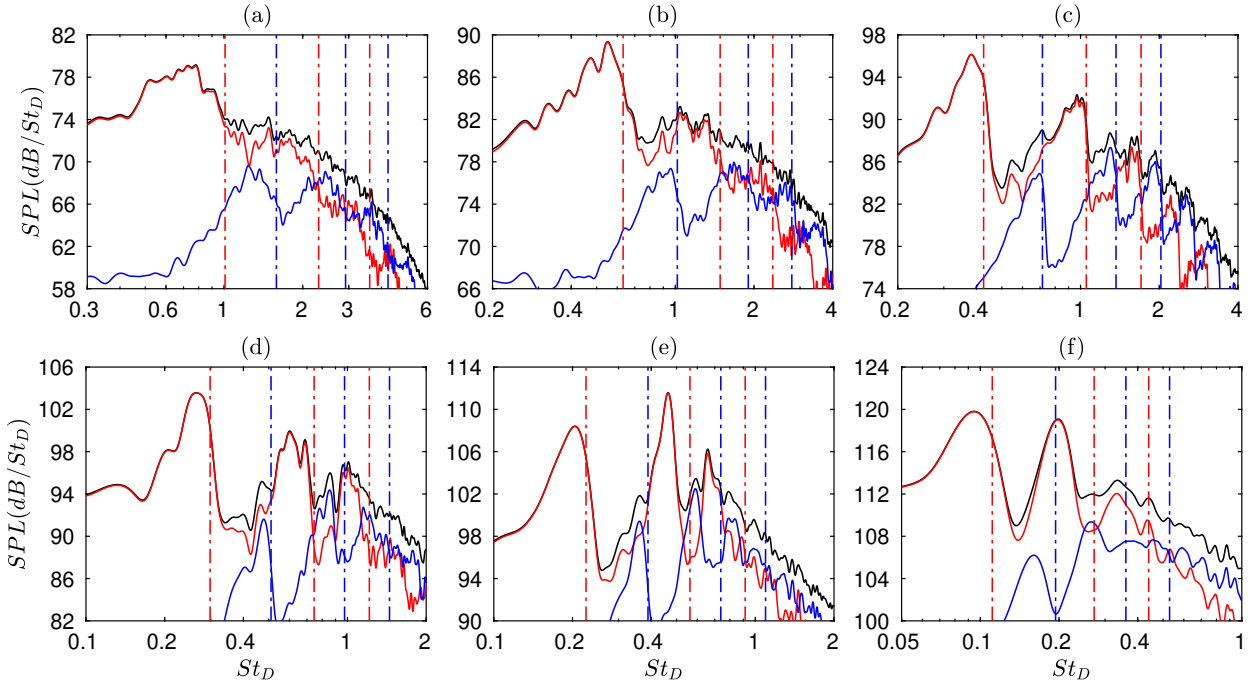

Fig. 12 Sound pressure levels at ϕ = 175° for (a) M = 0.60, (b) M = 0.75, (c) M = 0.90, (d) M = 1.10, (e) M = 1.30 and (f) M = 2: ——— total, n_θ = ——— 0, ——— 1, ——— 2, ——— 3, ——— 4 and ——— 5; (dash-dotted) cutoff frequencies of free-stream guided jet modes (n_θ = 0 – 1, n_r = 1 – 3).

exist, at a larger angle. For $n_\theta = 1$, for instance, the maximum is located at $\phi = 162^o$ for $n_r = 1$ but at $\phi = 173^o$ for $n_r = 3$ in figure 13(b). For $n_\theta = 0$, moreover, the level growth rates at $\phi \geq 165^o$ are higher for $n_r = 2$ and 3 than for $n_r = 1$ in figure 13(a), reducing the gap between the peak amplitudes by 6 dB between $\phi = 160^o$ and 179^o. Thus, the contributions of the radial guided jet modes $n_r \geq 2$ to the sound spectra get closer to those of the first radial modes, and even exceed them in some cases as in figure 12(e), as the radiation angle tends to 180^o.

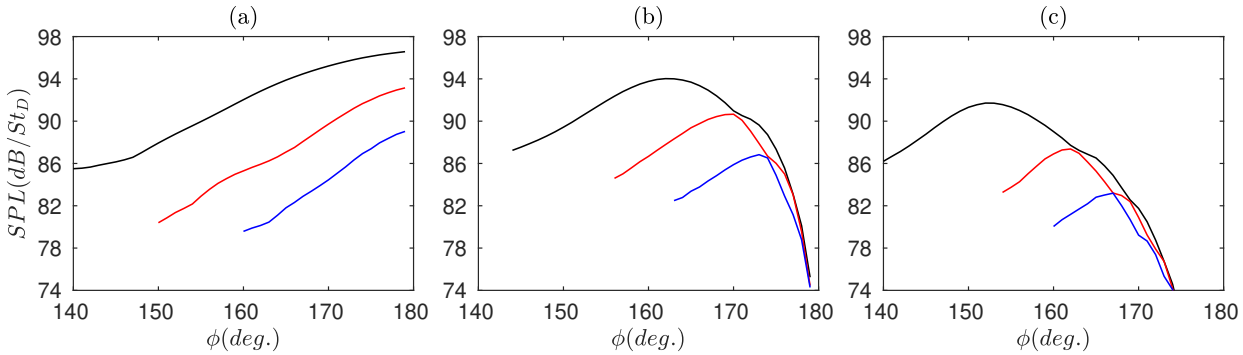

Fig. 13 Sound pressure levels at the peaks associated with the free-stream upstream-propagating guided jet waves of modes ($n_\theta = 0-2$, $n_r = 1-3$) for M = 0.90: (a) $n_\theta = 0$, (b) $n_\theta = 1$ and (c) $n_\theta = 2$; $n_r =$ ——— 1, ——— 2 and ——— 3.

IV. Conclusion

In this paper, acoustic tones have been shown to emerge in the far field of high subsonic and of screeching or non-screeching, supersonic jets for very large angles relative to the flow direction based on data from both experiments and large-eddy simulations, over the Mach number range $0.60 \leq \mathrm{M} \leq 2$ and for a wide variety of nozzle-exit boundary-layer conditions. As for the near-nozzle tones identified and described in previous studies, these far-field tones are due to the presence of upstream-propagating guided jet waves with a non-negligible support outside of the flow within limited frequency bands. Overall, the tones have significant levels for radiation angles $\phi \gtrsim 150^o$. As the angle increases, they strengthen and are related to lower azimuthal and higher radial guided jet modes. In the upstream direction, in particular, strong peaks associated with the axisymmetric mode predominate in the far-field sound spectra over the entire Mach number range considered.

Appendix

To briefly reexamine the far field spectra obtained in the experiments [24] in the light of our current knowledge on the near-nozzle acoustic tones, the spectra measured for the jet at M = 0.90 for $\phi = 30^o$, 60^o, 90^o, 120^o and 150^o are represented in figure 14, scaled in amplitude at a distance of $R = 75D$ from the nozzle. The cuttoff frequencies of the free-stream upstream-propagating guided jet modes ($n_\theta = 0-8$, $n_r = 1$) predicted using the vortex-sheet model are also shown. As expected, no tone emerge in the spectra for $\phi \leq 120^o$. More surprisingly, small undulations can

be detected in the spectra around the cuttoff frequencies of the guided jet modes. This is in particularly the case at Strouhal numbers $\mathrm{St}_D \simeq 2$, as was noticed by Zaman and Fagan [23] for jets at similar Mach numbers. Given the fact that such undulations are not found in the LES far-field spectra in Bogey [14], for instance, they may be due to unwanted acoustic reflections in the experiments.

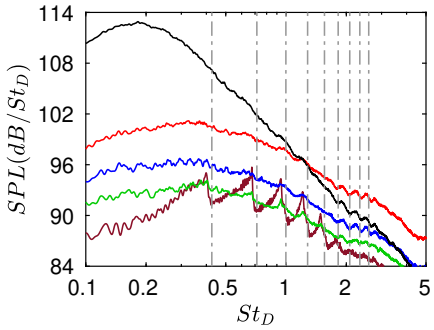

Fig. 14 Sound pressure levels at ϕ = ——— 30°, ——— 60°, ——— 90°, ——— 120° and ——— 150° for M = 0.90; – · – · cutoff frequencies of the free-stream guided jet modes ($n_\theta = 0-8$, $n_r = 1$).

Acknowledgments

This work was granted access to the HPC resources of PMCS2I (Pôle de Modélisation et de Calcul en Sciences de l'Ingénieur et de l'Information) of Ecole Centrale de Lyon, PSMN (Pôle Scientifique de Modélisation Numérique) of ENS de Lyon and P2CHPD (Pôle de Calcul Hautes Performances Dédiés) of Université Lyon I, members of FLMSN (Fédération Lyonnaise de Modélisation et Sciences Numériques), partner of EQUIPEX EQUIP@MESO, and to the resources of CINES (Centre Informatique National de l'Enseignement Supérieur) and IDRIS (Institut du Développement et des Ressources en Informatique Scientifique) under the allocation 2020-2a0204 made by GENCI (Grand Equipement National de Calcul Intensif). It was performed within the framework of the LABEX CeLyA (ANR-10-LABX-0060) of Université de Lyon, within the program *Investissements d'Avenir* (ANR-16-IDEX-0005) operated by the French National Research Agency (ANR). The author is also grateful to Etienne Spieser for discussions on the measurements.

References

[1] Norum, T. D., and Seiner, J. M., "Measurements of mean static pressure and far field acoustics of shock-containing supersonic jet," Tech. Rep. 84521, NASA TM, 1982.

[2] Norum, T. D., "Screech suppression in supersonic jets," *AIAA J.*, Vol. 21, No. 2, 1983, pp. 235–240. doi:10.2514/3.8059.

[3] Zaman, K. B. M. Q., and Yu, J. C., "Power spectral density of subsonic jet noise," *J. Sound Vib.*, Vol. 98, No. 4, 1985, pp. 519–537. doi:10.1016/0022-460X(85)90259-7.

[4] Lush, P. A., "Measurements of subsonic jet noise and comparison with theory," *J. Fluid Mech.*, Vol. 46, No. 3, 1971, pp. 477–500. doi:10.1017/S002211207100065X.

[5] Mollo-Christensen, E., Kolpin, M. A., and Martucelli, J. R., "Experiments on jet flows and jet noise far-field spectra and directivity patterns," *J. Fluid Mech.*, Vol. 18, No. 2, 1964, pp. 285–301. doi:10.1017/S0022112064000209.

[6] Ahuja, K. K., and Bushell, K. W., "An experimental study of subsonic jet noise and comparison with theory," *J. Sound Vib.*, Vol. 30, No. 3, 1973, pp. 317–341. doi:10.1016/S0022-460X(73)80242-1.

[7] Brown, C., and Bridges, J., "Small hot jet acoustic rig validation," Tech. Rep. 2006-214234, NASA TM, 2006.

[8] Tam, C. K. W., Viswanathan, K., Ahuja, K. K., and Panda, J., "The sources of jet noise: experimental evidence," *J. Fluid Mech.*, Vol. 615, 2008, pp. 253–292. doi:10.1017/S0022112008003704.

[9] Tanna, H. K., "An experimental study of jet noise. Part I: Turbulent mixing noise," *J. Sound Vib.*, Vol. 50, No. 3, 1977, pp. 405–428. doi:10.1016/0022-460X(77)90493-X.

[10] Viswanathan, K., "Instrumentation considerations for accurate jet noise measurements," *AIAA J.*, Vol. 44, No. 6, 2006, pp. 1137–1149. doi:10.2514/1.13518.

[11] Suzuki, T., and Colonius, T., "Instability waves in a subsonic round jet detected using a near-field phased microphone array," *J. Fluid Mech.*, Vol. 565, 2006, pp. 197–226. doi:10.1017/S0022112006001613.

[12] Towne, A., Cavalieri, A. V. G., Jordan, P., Colonius, T., Schmidt, O., Jaunet, V., and Brès, G. A., "Acoustic resonance in the potential core of subsonic jets," *J. Fluid Mech.*, Vol. 825, 2017, pp. 1113–1152. doi:10.1017/jfm.2017.346.

[13] Brès, G. A., Jordan, P., Jaunet, V., Le Rallic, M., Cavalieri, A. V. G., Towne, A., Lele, S. K., Colonius, T., and Schmidt, O. T., "Importance of the nozzle-exit boundary-layer state in subsonic turbulent jets," *J. Fluid Mech.*, Vol. 851, 2018, pp. 83–124. doi:10.1017/jfm.2018.476.

[14] Bogey, C., "Acoustic tones in the near-nozzle region of jets: characteristics and variations between Mach numbers 0.5 and 2," *J. Fluid Mech.*, Vol. 921, 2021, p. A3. doi:10.1017/jfm.2021.426.

[15] Tam, C. K. W., and Hu, F. Q., "On the three families of instability waves of high-speed jets," *J. Fluid Mech.*, Vol. 201, 1989, pp. 447–483. doi:10.1017/S002211208900100X.

[16] Bogey, C., and Gojon, R., "Feedback loop and upwind-propagating waves in ideally-expanded supersonic impinging round jets," *J. Fluid Mech.*, Vol. 823, 2017, pp. 562–591. doi:10.1017/jfm.2017.334.

[17] Jordan, P., Jaunet, V., Towne, A., Cavalieri, A. V. G., Colonius, T., Schmidt, O., and Agarwal, A., "Jet–flap interaction tones," *J. Fluid Mech.*, Vol. 853, 2018, pp. 333–358. doi:10.1017/jfm.2018.566.

[18] Gojon, R., Bogey, C., and Mihaescu, M., "Oscillation modes in screeching jets," *AIAA J.*, Vol. 56, No. 7, 2018, pp. 2918–2924. doi:10.2514/1.J056936.

[19] Edgington-Mitchell, D., Jaunet, V., Jordan, P., Towne, A., Soria, J., and Honnery, D., "Upstream-travelling acoustic jet modes as a closure mechanism for screech," *J. Fluid Mech.*, Vol. 855, 2018, p. R1. doi:10.1017/jfm.2018.642.

[20] Mancinelli, M., Jaunet, V., Jordan, P., and Towne, A., "Screech-tone prediction using upstream-travelling jet modes," *Exp Fluids*, Vol. 60, No. 1, 2019, p. 22. doi:10.1007/s00348-018-2673-2.

[21] Edgington-Mitchell, D., "Aeroacoustic resonance and self-excitation in screeching and impinging supersonic jets - A review," *Int. J. Aeroacoust.*, Vol. 18, No. 2-3, 2019, pp. 118–188. doi:10.1177/1475472X19834521.

[22] Jaunet, V., Jordan, P., Cavalieri, A. V. G., Towne, A., Colonius, T., Schmidt, O., and Brès, G. A., "Tonal dynamics and sound in free and installed turbulent jets," Tech. Rep. 2016-3016, AIAA Paper, 2016. doi:10.2514/6.2016-3016.

[23] Zaman, K. B. M. Q., and Fagan, A. F., "Near-exit pressure fluctuations in jets from circular and rectangular nozzles," Tech. Rep. 2019-220383, NASA TM, 2019.

[24] Bogey, C., Barré, S., Fleury, V., Bailly, C., and Juvé, D., "Experimental study of the spectral properties of near-field and far-field jet noise," *Int. J. Aeroacoust.*, Vol. 6, No. 2, 2007, pp. 73–92. doi:10.1260/147547207781041868.

[25] Zaman, K. B. M. Q., "Effect of initial condition on subsonic jet noise," *AIAA J.*, Vol. 23, No. 9, 1985, pp. 1370–1373. doi:10.2514/3.9094.

[26] Ahuja, K. K., Tester, B. J., and Tanna, H. K., "Calculation of far field jet noise spectra from near field measurements with true source location," *J. Sound Vib.*, Vol. 116, No. 3, 1987, pp. 415–426. doi:10.1016/S0022-460X(87)81374-3.

[27] Viswanathan, K., "Distributions of noise sources in heated and cold jets: are they different?" *Int. J. Aeroacoust.*, Vol. 9, No. 4-5, 2010, pp. 589–625. doi:10.1260/1475-472X.9.4-5.589.

[28] Seiner, J. M., "Advances in high speed jet aeroacoustics," Tech. Rep. 84-2275, AIAA Paper, 1984. doi:10.2514/6.1984-2275.

[29] Bogey, C., Marsden, O., and Bailly, C., "Large-Eddy Simulation of the flow and acoustic fields of a Reynolds number 10^5 subsonic jet with tripped exit boundary layers," *Phys. Fluids*, Vol. 23, No. 3, 2011, p. 035104. doi:10.1063/1.3555634.

[30] Bogey, C., and Bailly, C., "A family of low dispersive and low dissipative explicit schemes for flow and noise computations," *J. Comput. Phys.*, Vol. 194, No. 1, 2004, pp. 194–214. doi:10.1016/j.jcp.2003.09.003.

[31] Fauconnier, D., Bogey, C., and Dick, E., "On the performance of relaxation filtering for large-eddy simulation." *J. Turbulence*, Vol. 14, No. 1, 2013, pp. 22–49. doi:10.1080/14685248.2012.740567.

[32] Kremer, F., and Bogey, C., "Large-eddy simulation of turbulent channel flow using relaxation filtering: Resolution requirement and Reynolds number effects," *Comput. Fluids*, Vol. 116, 2015, pp. 17–28. doi:10.1016/j.compfluid.2015.03.026.

[33] Tam, C. K. W., and Dong, Z., "Radiation and outflow boundary conditions for direct computation of acoustic and flow disturbances in a nonuniform mean flow," *J. Comput. Acous.*, Vol. 4, No. 2, 1996, pp. 175–201. doi:10.1142/S0218396X96000040.

[34] Bogey, C., "Grid sensitivity of flow field and noise of high-Reynolds-number jets computed by large-eddy simulation," *Int. J. Aeroacoust.*, Vol. 17, No. 4-5, 2018, pp. 399–424. doi:10.1177/1475472X18778287.

[35] Bogey, C., and Sabatini, R., "Effects of nozzle-exit boundary-layer profile on the initial shear-layer instability, flow field and noise of subsonic jets," *J. Fluid Mech.*, Vol. 876, 2019, pp. 288–325. doi:10.1017/jfm.2019.546.

[36] Bogey, C., "Generation of excess noise by jets with highly disturbed laminar boundary-layer profiles," *AIAA J.*, Vol. 59, No. 2, 2021, pp. 569–579. doi:10.2514/1.J059610.

[37] Pineau, P., and Bogey, C., "Numerical investigation of wave steepening and shock coalescence near a cold Mach 3 jet," *J. Acoust. Soc. Am.*, Vol. 149, No. 1, 2021, pp. 357–370. doi:10.1121/10.0003343.

[38] Bogey, C., de Cacqueray, N., and Bailly, C., "Finite differences for coarse azimuthal discretization and for reduction of effective resolution near origin of cylindrical flow equations," *J. Comput. Phys.*, Vol. 230, No. 4, 2011, pp. 1134–1146. doi:10.1016/j.jcp.2010.10.031.

[39] Bogey, C., Marsden, O., and Bailly, C., "Influence of initial turbulence level on the flow and sound fields of a subsonic jet at a diameter-based Reynolds number of 10^5," *J. Fluid Mech.*, Vol. 701, 2012, pp. 352–385. doi:10.1017/jfm.2012.162.

[40] Bridges, J., and Brown, C. A., "Validation of the small hot jet acoustic rig for aeroacoustic research," Tech. Rep. 2005-2846, AIAA Paper, 2005. doi:10.2514/6.2005-2846.

[41] Juvé, D., Sunyach, M., and Comte-Bellot, G., "Filtered azimuthal correlations in the acoustic far field of a subsonic jet," *AIAA J.*, Vol. 17, No. 1, 1979, pp. 112–113. doi:10.2514/3.61076.

[42] Cavalieri, A. V. G., Jordan, P., Colonius, T., and Gervais, Y., "Axisymmetric superdirectivity in subsonic jets," *J. Fluid Mech.*, Vol. 704, 2012, pp. 388–420. doi:10.1017/jfm.2012.247.

[43] Lighthill, M. J., "On sound generated aerodynamically I. General theory," *Proc. Roy. Soc. A*, Vol. 211, No. 1107, 1952, pp. 564–587. doi:10.1098/rspa.1952.0060.

[44] Ffowcs Williams, J. E., "The noise from turbulence convected at high speed," *Phil. Trans. R. Soc. Lond. A*, Vol. 255, No. 1061, 1963, pp. 469–503. doi:10.1098/rsta.1963.0010.